Precision Experiments on Muonium. I. Determination of the Muonium Hyperfine Splitting in Low-Pressure Argon from a Field-Independent Zeeman Transition*

R. D. Ehrlich,† H. Hofer,‡ A. Magnon,§ D. Y. Stowell,‖ R. A. Swanson,** and V. L. Telegdi
The Enrico Fermi Institute and Department of Physics, The University of Chicago, Chicago, Illinois 60637
(Received 30 December 1971)

The ground-state hyperfine interval $\Delta\nu$ of muonium has been redetermined in argon by measuring the $(1,1) \leftrightarrow (1,0)$ Zeeman frequency ν_1 at that external field value where $\partial\nu_1/\partial B = 0$. The measurements were performed with good statistics at much lower pressures than heretofore, greatly reducing uncertainties in extrapolating to zero pressure. Our value, $\Delta\nu(0) = 4463.313\,(18)$, disagrees with the linearly extrapolated values found in higher-pressure Ar and Kr by Crane *et al.* However, a new interpretation, namely, a pressure extrapolation based on a quadratic function with the linear coefficient fixed at the "atomic" value (i.e., assumption of no isotope dependence in the linear pressure shift), results in consistency between all present (data published before April, 1971) determinations of $\Delta\nu$.

I. INTRODUCTION

We are conducting at the University of Chicago a series of experiments on muonium, the hydrogenlike atomic system having a positive muon as the nucleus. The goals of the series include improved measurements of the ground-state hyperfine interval $\Delta\nu$ and of the muon magnetic moment. Both quantities can be determined from frequencies of Zeeman transitions [though the hyperfine (hf) interval may be measured directly]. These two quantities, both interesting in their own right, allow a very accurate independent determination of the fine-structure constant α; on the other hand, assuming α as known, these measurements afford a rather stringent test of quantum electrodynamics (QED).

The experiment described here was the first in this series, and it had two goals: (a) determination of the hyperfine interval, from a high-field Zeeman transition, at sufficiently low pressure to minimize the extrapolation difficulties (i.e., systematic errors) which plagued previous determinations, and (b) the development of novel experimental techniques to be used in subsequent experiments. This second point deserves emphasis since the following experiments will determine the hf interval with an accuracy greater than the present one.

All precision experiments on muonium may in general terms be described as follows: Polarized muons are stopped in a noble gas, where they capture electrons and form muonium in its ground state with the muon polarization partially preserved. An applied microwave (rf) field causes, when at resonance, a transition involving spin flip of the muon. The transition frequency is determined by measuring the change in the positron decay asymmetry which accompanies the spin flip.

Following their discovery of muonium, the Yale group determined $\Delta\nu$ in a series of experiments of increasing accuracy. First[1-3] the Zeeman transition $(F, M_F)(1,1) \leftrightarrow (1,0)$ was measured in argon at $B \simeq 5000$ G ("high-field experiment") at pressures from 10 to 70 atm. The measured frequencies suffered the well-known pressure shift (due to muonium-Ar collisions); they were linearly extrapolated to zero pressure, yielding

$$\Delta\nu(0) = 4463.15\,(06)\ \text{MHz}\quad (13\ \text{ppm}).$$

Next $\Delta\nu$ was determined directly in zero and low (~ 3 G) magnetic fields, in Ar from 30 to 108 atm[4,5] and in Kr from 6 to 73 atm.[5] The values obtained, using again linear extrapolation, were

$$\Delta\nu(0) = 4463.220\,(20)\ \text{MHz}\quad (\text{Ar},\ 4.5\ \text{ppm})$$

and

$$\Delta\nu(0) = 4463.262\,(12)\ \text{MHz}\quad (\text{Kr},\ 2.7\ \text{ppm}).$$

Ideally, an extrapolation in either gas should yield the same "vacuum" value $\Delta\nu(0)$; an error, expanded to allow for the poor agreement between the two above results, was attached to their weighted mean, yielding 4463.249 (31) MHz (7 ppm).

The assumption that the pressure shift of $\Delta\nu$ is a *linear* function of density over the pressure range involved in the Yale experiments has been open for question for some time,[6] and the Ar-Kr discrepancy discussed above could perhaps be attributed to an additional *quadratic* term in the density dependence. One of the prime aims of the present work was to minimize the importance of the pressure shift as a source of systematic error. To this effect, this present experiment was designed to measure $\Delta\nu$ at 5 atm of Ar, the lowest pressure used to date. For this pressure p, the *total* shift of $\Delta\nu(p)$ from $\Delta\nu(0)$ is less than the difference between the extrapolated Yale Ar and Kr values.

The possibilities of running the low-density tar-

gets are limited since not only the absolute stop rate decreases with the density of the gas, but so does the ratio of muons stopping in the useful gas volume to those stopping in the surrounding walls.

From the point of view of wall stops at least, a high-field approach is preferable to the zero-field method, because a strong magnetic field along the direction of incidence of the stopping muon beam tends to counteract the radial spreading out caused by multiple scattering. On the other hand, it appears harder to use an rf cavity of large volume in the high-field case because of field homogeneity requirements.

The present work is again a measurement of the $(1,1)\leftrightarrow(1,0)$ Zeeman frequency ν_1, but with several experimental improvements: (a) the external field chosen to have that "magic" value (11.3 kG) where $\partial\nu_1/\partial B=0$, thus significantly alleviating the homogeneity requirements; (b) discriminating against muon stops outside the gas volume of interest by means of proportional counters located *within* that volume; (c) adopting a mode (TM_{210}) which allows both for a large rf-cavity diameter [thanks to (a)] and for a more uniform rf power throughout the volume of interest; (d) measuring the time-dependent evolution of the rf-induced change in muon polarization rather than only the net change integrated over the observation time. Each of these points will be discussed more fully in the body of the paper.

II. PRINCIPLE OF EXPERIMENT

The essence of the experiment is to measure the frequency ν_1 corresponding to the Zeeman transition (F,M_F) $(1,1)\leftrightarrow(1,0)$. Inasmuch as the underlying theory has already been repeatedly described[1] in connection with the Yale high-field work of which ours is but an extension, we shall keep the discussion extremely brief and describe only novel points in detail.

The Breit-Rabi formula gives

$$\nu_1(x)=(\tfrac{1}{2}\Delta\nu)\,[1-(1+x^2)^{1/2}+x(1-2G)]\,, \qquad (1)$$

where $\Delta\nu=\Delta\nu(p)$ is the hf splitting at the operating density (or, loosely speaking, pressure) of the host gas and[1]

$$\Delta\nu(0)=(\tfrac{16}{3}\alpha^2 R_\infty c g_e g'_\mu)(1+m_e/m_\mu)^{-3}(1+\mathcal{E}_{\rm QED})\,, \qquad (2)$$

$$\mathcal{E}_{\rm QED}=\tfrac{3}{2}\alpha^2+\epsilon_1+\epsilon_2+\epsilon_3+\delta_{\mu1}+\delta_{\mu2}\,,$$

$$\epsilon_1=\alpha^2(\ln 2-\tfrac{5}{2})\,,$$

$$\epsilon_2=-\left(\frac{8\alpha^3}{3\pi}\right)\ln\alpha\,(\ln\alpha+\tfrac{281}{480}-\ln 4)\,,$$

$$\epsilon_3=(\alpha^3/\pi)18.4\,,$$

$$\delta_{\mu1}=\frac{-(3\alpha/\pi)(m_e/m_\mu)\ln(m_e/m_\mu)}{1-(m_e/m_\mu)^2}\,,$$

$$\delta_{\mu2}=\tfrac{9}{2}\alpha^2(\ln\alpha^{-1})\left(\frac{m_e}{m_\mu}\right)\left(1+\frac{m_e}{m_\mu}\right)^{-2}\,,$$

where the leading factor is the nonrelativistic Fermi formula, the second is the simple reduced mass correction and, among the terms called $\mathcal{E}_{\rm QED}$, $\frac{3}{2}\alpha^2=79.88$ ppm is the relativistic correction to the Schrödinger wave function (strictly speaking, not QED), $\epsilon_1=-96.22$ ppm, $\epsilon_2=-9.29$ ppm, and $\epsilon_3=2.28$ ppm are virtual radiative corrections, and $\delta_{\mu1}=-179.7$ ppm as well as $\delta_{\mu2}=5.6$ ppm are relativistic recoil corrections, of which the second one has become available just recently.[7] The total $\mathcal{E}_{\rm QED}$ correction is [1 − 197.45 ppm]

$$G=g'_\mu[M]/(g'_\mu[M]-g_j)\,,$$

where g'_μ is $g_\mu(m_e/m_\mu)$, and $g'_\mu[M]$ the corresponding quantity corrected for the reduction of the external field B by the diamagnetism of the electron in muonium[8]; $g'_\mu[M]=g'_\mu(1-\frac{1}{3}\alpha^2)$,

$$g_j=g \text{ factor of the bound electron}=g_e(1-\tfrac{1}{3}\alpha^2)\,.$$

Note that $G\approx g'_\mu/g_e\approx(m_e/m_\mu)\approx\frac{1}{200}$.

In (1) the external field B is measured in dimensionless "Zeeman units," i.e.,

$$x=\frac{(\mu_B B)}{(h\Delta\nu)(g_j-g'_\mu[M])}\approx\frac{2\mu_B B}{h\Delta\nu}=\frac{B[\mathrm{G}]}{1583}\,. \qquad (3)$$

It is an essential point of the present approach that ν_1 is determined at or near that "magic" field value x_0 where this frequency is, to first order, *field independent*:

$$\nu_1(x)=\nu_1(x_0)+\frac{1}{2}\frac{\partial^2\nu}{\partial x^2}(\Delta x)^2\,.$$

Differentiating (1), the condition $\partial\nu/\partial x|_{x_0}=0$ yields

$$x_0=x_0(G)=(1-2G)/2[G(1-G)]^{1/2}=7.1549$$

corresponding to 11 327 G. Note that ν_1 is maximum at x_0. The existence of this maximum is intuitively obvious from the fact that the levels (1, 1) and (1, 0) must *cross* in the extremely high fields where the level with both moments opposite $\vec{B}$ ($\vec{S}_e\cdot\hat{z}=\frac{1}{2}$, $\vec{S}_\mu\cdot\hat{z}=-\frac{1}{2}$) lies highest.

The vanishing of the linear field dependence of ν_1 near x_0 is of practical usefulness only to the extent that the quadratic (and higher) coefficients are small. Fortunately, this is indeed the case:

$$\frac{\Delta\nu_1}{\nu_1(x_0)}\cong\frac{1}{2}\frac{\partial^2\nu_1}{\partial x^2}\frac{\Delta x^2}{\nu_1(x_0)}\approx\frac{1}{2x_0}\left(\frac{\Delta x}{x}\right)^2\,,$$

so that an rms variation (in space or time) of 1% in the external field produces only a shift of 7 ppm in ν_1. Obviously any departure of B from its "magic" value always calls for a positive correction to the measured ν_1.

Since $x_0=x_0(G)$, $\nu_1(x_0)$ depends on $\Delta\nu$ only through G:

$$\nu_1(x_0) = (\tfrac{1}{2}\Delta\nu)\{1 - 2[G(1-G)]^{1/2}\} \quad (4)$$

and not explicitly on the external field B. It is in fact possible to avoid accurate measurements of B by simply varying the field and locating the maximum ν_1.[9] Numerically, with $g'_\mu[M]/g_j = g'_\mu/g_e = 206.770\,(65)$[10]:

$$\nu_1 = [0.43079129\,(44)]\Delta\nu \ . \quad (4a)$$

Thus the G-dependent part of ν_1 in (4) amounts to about 14%, and an uncertainty of, say, 10 ppm in g'_μ/g_j contributes only an uncertainty of 1.43 ppm to $\Delta\nu$.

It may be of interest to compare the field dependence of the original high-field experiment[1,3] with the present approach.

Clearly for a fully linear Zeeman effect ($x \to 0$), one would have $\delta\nu_1/\nu_1 = \delta x/x$. Near $x = 3.12$, the value used in Ref. 2, one finds from (3)

$$\delta\nu_1/\nu_1 = (1/x)\ (\delta x/x) + 2x(\delta x/x)^2 \ ,$$

i.e., the linear dependence is only a factor 3 improved over the worst case, and an rms variation of 1% would induce a quadratic shift of 300 ppm!

We now turn to the signal, i.e., the change in muon polarization induced by the transition (1, 1) $\leftrightarrow$(1, 0). In terms of muon and electron spinors, the Zeeman eigenstates (in an external field along z) are

$$|1,1\rangle = |\alpha_e\alpha_\mu\rangle \ , \quad |1,-1\rangle = |\beta_e\beta_\mu\rangle \ ,$$
$$|1,0\rangle = c\,|\alpha_e\beta_\mu\rangle + s\,|\beta_e\alpha_\mu\rangle \to |\alpha_e\beta_\mu\rangle \quad \text{as } B \to \infty \ ,$$
$$|0,0\rangle = c\,|\beta_e\alpha_\mu\rangle - s\,|\alpha_e\beta_\mu\rangle \to |\beta_e\alpha_\mu\rangle \quad \text{as } B \to \infty \ ,$$

with $c(s) = 2^{-1/2}\,[1 + (-)\epsilon(x)]$, $\epsilon = x/(1+x^2)$. At the "magic" field, $\epsilon \approx 0.14$ and one is near the Paschen-Back limit indicated above by the arrows. Hence a muon beam initially polarized along $\vec{B}$ will form muonium almost entirely in the states $|1,1\rangle$ and $|0,0\rangle$ with equal probability, and the transition (1, 1) $\to$ (1, 0) will correspond to an almost *complete* muon spin flip. In this limit the transition probability in a linear rf field of frequency ω and amplitude $2B_1$ will be given *exactly* by the Majorana-Rabi formula for a free muon:

$$W_{\beta\alpha}(t) = (2b/\Omega)^2 \sin^2 \tfrac{1}{2}\Omega t \ , \quad (5)$$

where $\Omega^2 = (\Delta\omega)^2 + (2b)^2$, $\Delta\omega = \omega_0 - \omega$, and $2b = g'_\mu \mu_B B_1 = \omega_s$. [For actual calculations, one must use $2b = (c\,g'_\mu\,\mu_B + s\,g_J\,\mu_B)B_1$ rather than the free muon approximation given above.] $W_{\beta\alpha}(t)$ is the probability to find the spin "down" at a time t, given that it was with certainty "up" at $t = 0$. Clearly, we find

$$W(t) = N_\beta(t)/[N_\alpha(t) + N_\beta(t)] = N_\beta(t) \ ,$$

and the polarization has the time dependence

$$P(t) \equiv \langle\sigma_z(t)\rangle = N_\alpha(t) - N_\beta(t) = 1 - 2\,W_{\beta\alpha}$$
$$= 1 - (2b/\Omega)^2\,(1 - \cos\Omega t). \quad (6)$$

The meaning of (6) becomes particularly clear at resonance ($\Delta\omega = 0$, $\Omega = 2b = \omega_s$), where

$$P(t, \omega = \omega_0) = \cos\omega_s t \ , \quad (7)$$

i.e., the spin precesses about B_1. Consider first only the muonium atoms formed in the (1, 1) state [the 50% in the (0, 0) state are unaffected by the microwaves of frequency $\omega_0 = 2\pi\nu_1$]. In the absence of microwaves, the decay positron rate is

$$N_{off}(t) = \lambda N_0 e^{-\lambda t}\,[1 + a\vec{P}(0)\cdot\hat{p}] \ , \quad (8)$$

where $\lambda = 1/\tau$ = decay rate, $\vec{p}$ is the positron momentum, $\hat{p} = \vec{p}/p$, and a is the muon decay asymmetry parameter. The latter depends on p; its unweighted average over the spectrum has the value $\bar{a} = \frac{1}{3}$. In the presence of microwaves, for the same muon intensity, one has

$$N_{on}(t) = \lambda N_0 e^{-\lambda t}\,[1 + a\vec{P}(t)\cdot\hat{p}] \ . \quad (9)$$

Hence

$$N_{off}(t) - N_{on}(t) = \lambda N_0 e^{-\lambda t} P_0 a\ \cos\theta(2b/\Omega)^2\,(1 - \cos\Omega t) \ .$$

This difference constitutes the time-dependent signal; in actual practice, it is preferable to normalize through N_{off}, i.e., to form

$$S(t; b, \Omega) = S(t; (\Delta\omega)^2, B_1^2) \equiv \frac{N_{off}(t) - N_{on}(t)}{N_{off}(t)}$$
$$= \frac{P_0 a\ \cos\theta(2b/\Omega)^2(1 - \cos\Omega t)}{1 \pm P_0 a} \ , \quad (10)$$

where we have emphasized the dependence on $(\Delta\omega)^2$ and on rf power (B_1^2). N_{on}, N_{off}, S as given above are valid for a pointlike positron detector viewing a point Q within the microwave cavity; for the actual signal, one has to average, for each Q, over the finite detector, and average the result over the cavity volume [where $B_1^2(Q)$ varies], weighting with the muon stop distribution:

$$S_{av}(t; (\Delta\omega)^2, B_1^2) = P_0\{[a\,\langle\cos\theta\rangle_{cav\ av}\langle(2b_1/\Omega)^2$$
$$\times(1 - \cos\Omega t)/(1 \pm a\,P_0\cos\theta)\rangle_{cav\ av}]_{det\ av}\}_{p\ av} \ ,$$
$$S_{av}(t; (\Delta\omega)^2, B_1^2) = \pm[P_0\bar{a}\epsilon/(1 \pm P_0\bar{a}\epsilon)]$$
$$\times\langle(2b/\Omega)^2(1 - \cos\Omega t)\rangle \ , \quad (11)$$

where $\bar{a}$ $(= \frac{1}{3})$ is the momentum averaged asymmetry parameter, and

$$\epsilon = \{[a(p)\,\langle\cos\theta\rangle_{cav\ av}]_{det\ av}\}_{r\ av}/\bar{a}$$

is the "asymmetry efficiency."

This effective separation of the averaging over space, and over rf power may be motivated, at least for this experiment, for each $\vec{p}$ as follows: Since the muons all stop within a radius smaller than that of the detectors, it is plausible (and verified by both Monte Carlo calculations and by di-

rect measurement) that the detector efficiency is primarily dependent upon the axial distance (z coordinate) from the detector and is insensitive to radial variations. The average over rf power will be a function of r only, since we are using the z-independent mode TM_{210}.

One can make the further hypothesis that averaging $\langle\ \rangle$ over rf power can be expressed in terms of an "effective power" $b^2_{\rm eff}$ [also, $\Omega_{\rm eff}=\Omega(b^2_{\rm eff})$]:

$$S_{\rm av}(t;(\Delta\omega)^2, B^2_{1\rm eff}) = \pm\frac{(P_0\bar{a}\epsilon)}{(1\pm P_0\bar{a}\epsilon)}\frac{4b^2_{\rm eff}}{\Omega^2_{\rm eff}}(1-\cos\Omega_{\rm eff}t)$$
$$= (\tfrac{1}{2}S_0)\frac{4b^2_{\rm eff}}{\Omega^2_{\rm eff}}(1-\cos\Omega_{\rm eff}t)\ , \quad (12)$$

where $S_0=\pm(P_0\bar{a}\epsilon)/(1\pm P_0\bar{a}\epsilon)$ is the peak height of the time-dependent signal at resonance.

Once the description of the data is in terms of an average rf field, i.e., Eq. (12) is accepted, the conventional analysis valid for a point source and a point detector may be taken over; hereafter, in referring to the time-dependent signal, we shall mean Eq. (12), and not carry the subscripts eff and av.

We next consider the signal obtained when the time distributions are not observed:

$$\begin{aligned}\bar{S} &= L(B_1^2, (\Delta\omega)^2)\\ &= [\textstyle\int_0^\infty N_{\rm off}(t)\,dt - \int_0^\infty N_{\rm on}(t)\,dt]/\int_0^\infty N_{\rm off}(t)\,dt\\ &= \textstyle\int_0^\infty S(t)N_{\rm off}(t)\,dt/\int_0^\infty N_{\rm off}(t)\,dt\\ &= (\tfrac{1}{2}S_0)(2b)^2/[(2b)^2+\lambda^2+(\Delta\omega)^2]\\ &= H(\tfrac{1}{2}\Gamma)^2/[(\tfrac{1}{2}\Gamma)^2+(\Delta\omega)^2]\ , \end{aligned} \quad (13)$$

where

$$\Gamma^2=(2b)^2+(\lambda^2)=\Gamma^2_{\rm rad}+\Gamma^2_0$$

and

$$H=(\tfrac{1}{2}S_0)(\Gamma_{\rm rad}/\Gamma)^2\ .$$

Equation (13) is now in a Lorentzian form, thus justifying the symbol L for the signal.

The statistical accuracy in determining the line center of a Lorentzian signal is proportional to H/Γ, which we shall use as a relative figure of merit. This quantity is given by

$$1/\sigma(\omega_0)\propto H/\Gamma=(\tfrac{1}{2}S_0)\,\Gamma^2_{\rm rad}/\Gamma^3$$

and attains a maximum for $\Gamma^2_{\rm rad}=2\Gamma^2_0$, a corresponding to $H=(\tfrac{1}{2}S_0)\frac{2}{3}$, $\Gamma=(3)^{1/2}\Gamma_0$, and a figure of merit of $0.39/\Gamma_0$. In view of unknown experimental difficulties, backgrounds, etc. we decided however to run at an average power producing 85% of the saturated signal, While this corresponds to a 40% larger Γ, the figure of merit $0.34/\Gamma_0$, yields a loss of statistical power of only 12%.

To gain a full understanding of the Lorentzian signal, the averages indicated in Eq. (11) were computed by a Monte Carlo technique. In a first step the asymmetry efficiency $\epsilon=\{[a(p)\langle\cos\theta\rangle_{\rm cav\ av}]_{\rm det\ av}\}_{p\ \rm av}/\bar{a}$ was determined throughout the cavity. For this, decay positrons were generated with a momentum and angular distribution given by the two-component neutrino theory[11] for muons "stopping" according to the measured distribution (see Sec. IV). The positron trajectories were tested for intercepting the telescopes, allowing for their helical character and the possibility of hitting the lateral cavity wall. The asymmetry efficiency was found to be $\epsilon=0.35\pm0.04$. Thus, we predict

$$H=\tfrac{1}{2}S_0\left(\frac{\Gamma_{\rm rad}}{\Gamma}\right)^2=\pm\left(\frac{P_0\bar{a}\epsilon}{1\pm P_0\bar{a}\epsilon}\right)0.85=\begin{cases}2.6\times10^{-2}(F)\\ -2.85\times10^{-2}(B)\end{cases},$$

where we used $P_0=\frac{0.55}{2}$, corresponding to the measured beam polarization (see Sec. IV) and to a loss of $\frac{1}{2}$ due to the rf-unaffected (0, 0) muonium atoms. An auxiliary calculation shows that averaging a constant muon stop distribution (out to the observed radius) over the B_1 field distribution of the TM_{210} rf-mode radius reduces the signal height by 7% with respect to that expected for a *constant* rf field, i.e., the above. Thus we predict a forward Lorentzian signal of 2.42%, a backward signal of 2.65%, and total signal of 5.1%. This prediction is to be compared with the corresponding experimental values (e.g., run 3, Sec. VI) of (2.3 ± 0.2)%, (3.08 ± 0.15)%, and $(5.38+0.25)$%. Thus there is excellent agreement between prediction and experiment; note that we assumed 100% muonium throughout.

One should notice that the asymmetry efficiency $\epsilon=0.35$ is quite low. This is due to the fact that the magnetic field increases the solid angle for the low-energy positrons more than for the high-energy ones, whereas $a(p)$ is such that the latter have the largest forward-backward asymmetry. There is, however, some compensation in statistical power through the larger *absolute* solid angle for positron detection. The Monte Carlo calculations mentioned above predict 0.26 ± 0.02 detected positrons/muon stop, whereas in the absence of a field this number would become 0.18.

In the preceding discussion of the signal it was implicitly assumed that the detection efficiency $g(t)$ of positrons is independent of the decay time, i.e., $g(t)=1$. The properties of the proportional counters used in this experiment (see Sec. III for details) were such that there *was* a slight dependence of this efficiency on decay time $[g(t)\neq ct]$. It is clear from the derivation of Eq. (12) that the time-dependent signal will *not* be affected by such effects; they will affect the integral signal $\bar{S}$ at most slightly, and in any case not affect its symmetry about ω_0. Furthermore, by forming the "pseudo-Lorentzian" integral signal discussed in Sec. VI, the influence of $g(t)$ drops out completely.

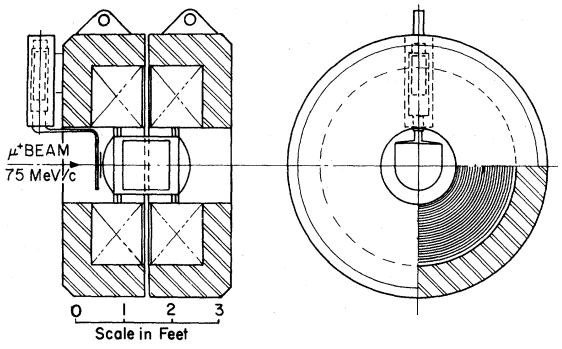

FIG. 1. Schematic drawing of magnet and muonium target. Only one counter is indicated to illustrate light-guide and shielding arrangement. Arrangement of all counters in magnet (Fig. 2) is similar.

Now we turn to the choice of the rf mode. It is natural to use a cylindrical rf cavity in this experiment, and one has to select an appropriate mode for the requisite frequency (~1922 MHz) for it. This choice was governed by the following considerations: (i) to have, within the limitations of the available magnet volume, as large a radius r as possible (in order to avoid muon stops in the cavity walls); (ii) to have as uniform radial distribution of rf power as possible (to increase the signal); and (iii) to use a z-independent mode (this makes the displacements of the end surfaces unimportant).

On the basis of these considerations, we adopted TM_{210}, corresponding to $r = 12.7$ cm (as compared to $r = 9.7$ cm for the TM_{110} mode used in the Yale high-field work[3]).

III. APPARATUS

Figures 1 and 2 show the experimental layout, Fig. 3 shows the electronic logic, and Fig. 4 is a timing diagram for that logic.

In general terms, our apparatus comprised (a) a large solenoid magnet, (b) the target, a pressure vessel containing the rf cavity; (c) a microwave system; (d) two scintillation counter telescopes to detect decay positrons; upstream and downstream from the target [$(\bar{3}56)$ and $(\bar{1}23\bar{5})$ in Fig. 2]; (e) a scintillation telescope to detect muons stops in the target [$(234\bar{5})$ in Fig. 2]; (f) two proportional counters to improve the spatial discrimination of the stop telescope (PC1 and PC2 in Fig. 2); (g) logic circuitry (Fig. 3) needed to run and to monitor the above; (h) gas circulating and purifying equipment; and (i) special counters and logic for mapping the stop distribution.

A. Magnet

A solenoidal bubble-chamber magnet, composed of two independent halves (see Fig. 1) with a free aperture of 15 in. diam was used. Its two halves were separated by a 1-in. gap to combine optimum uniformity with some radial accessibility to the target.

The field in the aperture was carefully mapped at approximately the required field (11.3 kG), by means of a nuclear resonance probe and showed primarily an axial variation with a maximum occurring at the midplane. The largest variation occurred along the magnet axis, corresponding to

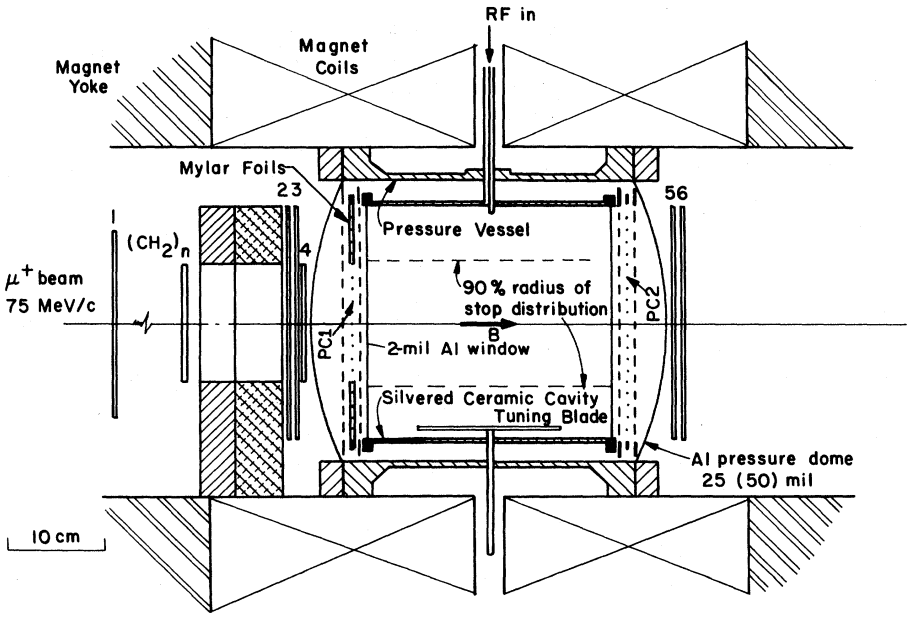

FIG. 2. Schematic cross section through the experimental setup. Scintillator dimensions are counter 1: 8×8 in.^{2} and 0.25 in. thick; counters 2, 3, 5 and 6: 10 in. diam and 0.188 in. thick; counter 4: 5 in. diam and 0.188 in. thick.

an rms inhomogeneity of 0.42% (equivalent to a 1.2-ppm shift in ν_1). Inasmuch as this inhomogeneity decreases radially whereas the number of muons stopping per annulus increases up to the "beam radius," 1.2 ppm constitutes an upper limit for the field-induced frequency shift. Accurate experimental knowledge of the product $\rho(\vec{r})\Omega(\vec{r})$ of the muon stop distribution $\rho(\vec{r})$ times the local solid angle $\Omega(\vec{r})$ (see Sec. IV) enabled us to reduce this error to 0.36% or 0.9 ppm. Finally, averaging over the (nonuniform) rf power in the cavity produces a 0.32% or 0.7-ppm shift.

The current was set to the value (1020 A) yielding the exact average B_0 by means of the nuclear resonance, and a temperature-compensated Hall probe was glued to the inner surface of the gap for future reference. The current was stabilized to 0.1% during the experiment, and no further adjustment was necessary.

B. Pressure Vessel and Gas System

The pressure vessel (see Fig. 1) was a 14-in.-long 0.25-in.-thick aluminum pipe of 12 in. o.d. Heavy flanges were welded to its ends to fasten the end windows, and reinforced ports were provided at various points on the midplane. Fed through individual ports and extending into the rf cavity were "air lines" (General Radio 874) leading to the rf drive and inspection loops, as well as a radially adjustable rod which carried the (quartz or Al) tuning blade (see Fig. 2). Two proportional-counter feedthroughs and a 1-in. pumping line went only into the pressure vessel proper.

Dome-shaped aluminum end windows were clamped to the flanges of the pressure vessel with appropriate rings, using titanium bolts torqued to 75 ft lb. 50-mil-thick windows were used in the high-pressure (17 atm) runs, while 25-mil-thick windows were employed at 5 atm.

The argon gas was continuously circulated through the target and a hot titanium purifier. The evacuation, circulation, and purification system was entirely similar to that of the Yale group,[2] and only relevant differences need be discussed here. The purifier was a vertical one, consisting of an Inconel pipe, a tightly fitted Alundum inner

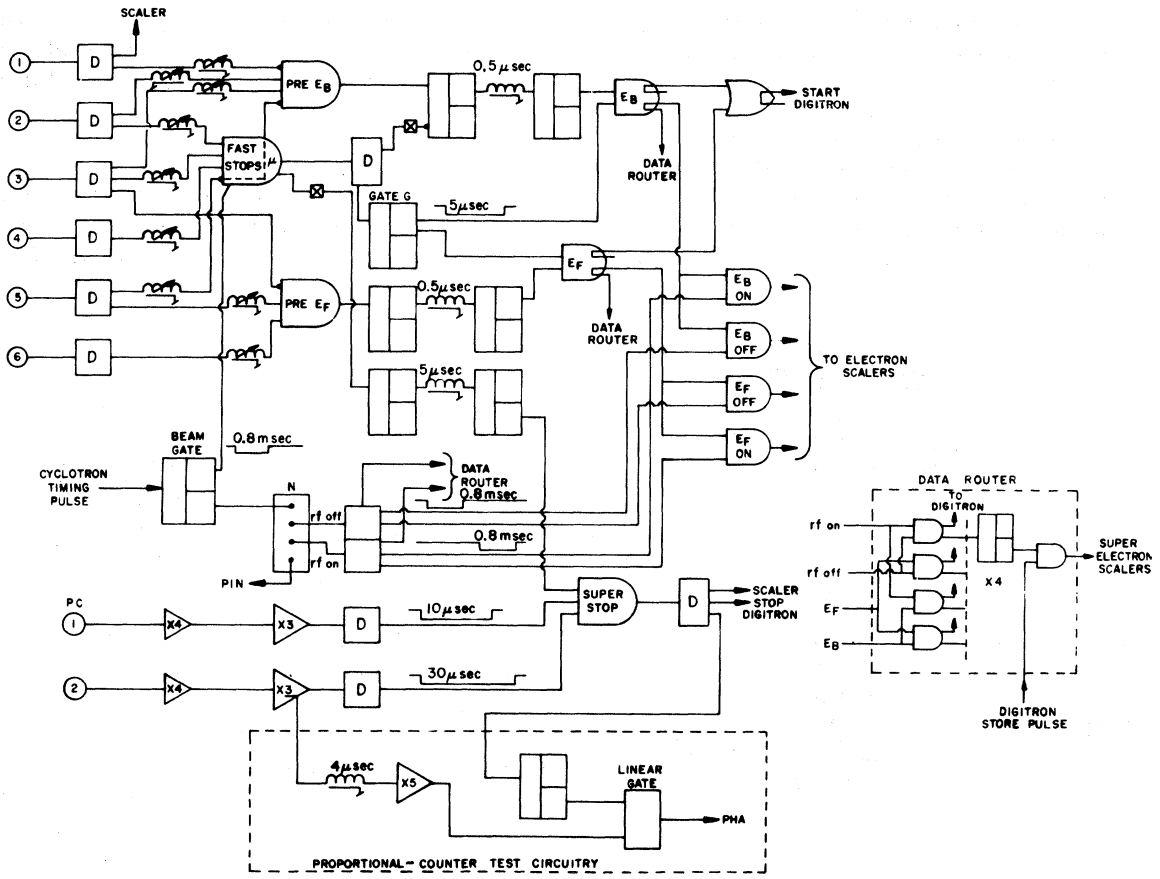

FIG. 3. Diagram of coincidence logic.

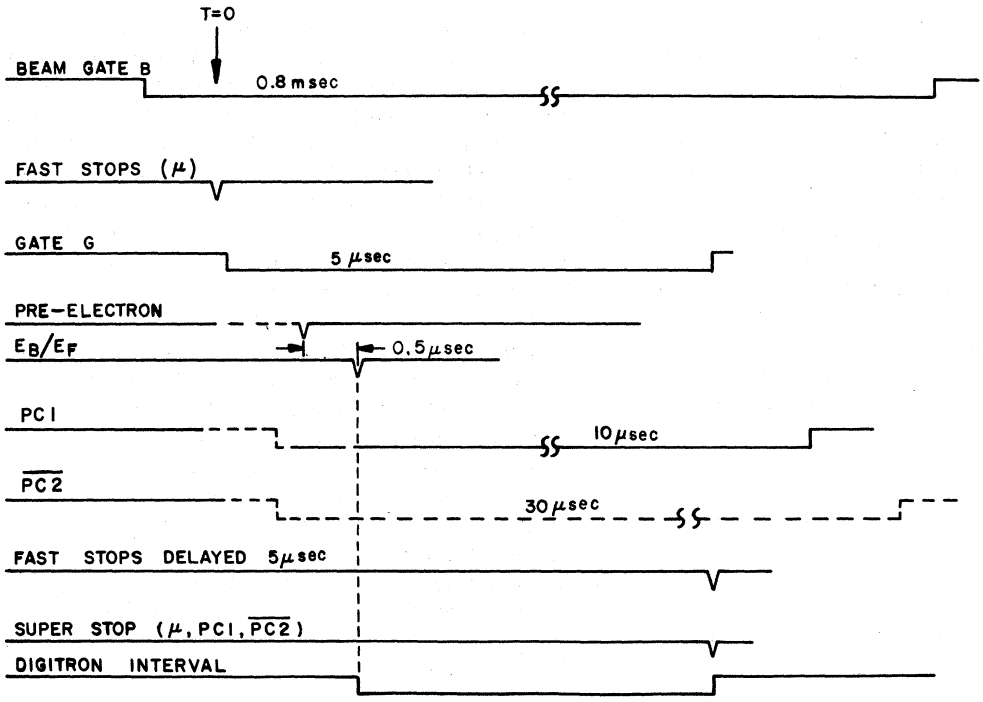

FIG. 4. Timing sequence of logic pulses in Fig. 3.

sleeve, and several tantalum baskets containing Ti powder. The pipe was heated to 850 °C at its center by an external oven and was water cooled at its ends.

After purification and cooling, the argon gas entered the cavity through the GR "air line" leading to the driving loop (see above), left the cavity through holes provided at the centers of its two end windows, and was finally returned to the purification system through a 1-in. pipe connected to the pressure vessel. The gas was circulated by means of a commercial pump (Whitey LP 10), at an estimated rate of 15 liter/hr.

C. Microwave System

The microwave system, schematically drawn in Fig. 5, was extremely straightforward. The source of rf power was a crystal-controlled os-

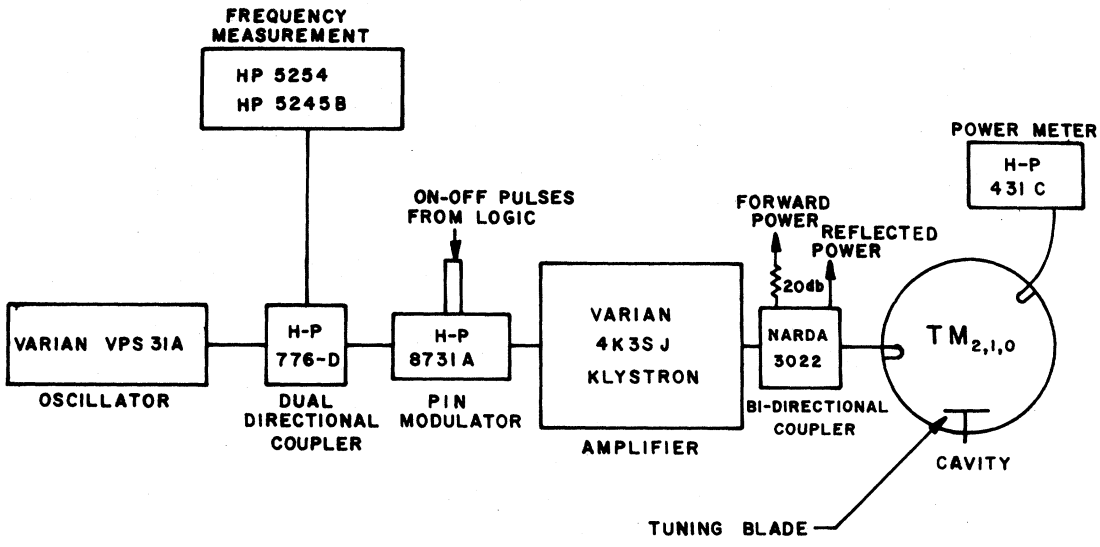

FIG. 5. Schematic diagram of microwave circuitry.

cillator followed by a klystron amplifier (Varian VPS, 31 A). The oscillator was thermostated and exhibited excellent stability (generally ±300 Hz, i.e., 0.15 ppm). The frequency was swept through the requisite range, about 300 kHz for each resonance, simply by manually changing crystals. A set of ten crystals with design frequencies spaced 150 kHz apart was provided within the thermostat, and fine adjustment within the range of each crystal was possible by retuning the oscillator.

The cavity consisted of a cylindrical body ($r = 12.7$ cm) and two end plates or "lids." The body was made of a special ceramic (Corning 9692) with a thermal expansion coefficient of $< 2 \times 10^{-6}/°C$ silvered on the appropriate surfaces; the use of this material eliminated the need for thermal stabilization against the rf-power dissipation in the cavity. The end plates consisted of aluminum rings over which 2-mil Al foil had been glued in a highly stretched condition, and which were clamped to the body. Firm electrical contact between these end plates and the body initially presented a problem. This was solved by burying an O-ring in the Al ring underneath the stretched foil, at a radius corresponding to the contact area of the body. The cavity had a reproducible (unloaded) Q of 40 000.

D. Scintillation Counters

Six scintillation counters were used in this experiment. Four (2, 3, 5 and 6 in Fig. 2) were of identical design, having an active approximately circular area of 5 in. radius, and were viewed through adiabatic light pipes which connected the scintillators located within the magnet to the photomultipliers (RCA 8575) placed outside it (see Fig. 1). Three concentric shields (two of soft iron, one of Molypermalloy) were sufficient to assure good operation.

Counter 4 was similar to these four counters, except that it had only a 5 in. diam. Its primary function was that of a collimation counter in the muon-stop telescope to be described below.

Counter 1, of 8×8 in. area, was located upstream of lead and aluminum beam collimators (5 in. diam) and served mainly to monitor the beam; it also had a function in the backward-positron telescope (see below).

E. Proportional Counters

The proportional counters were of a planar design, each counter consisting of three planes with wires spaced $\frac{3}{4}$ in. apart on the center plane (anode) and $\frac{1}{8}$ in. on the two outer ones (cathodes). The planes were $\frac{3}{8}$ in. apart. The anode wires were 1.2-mil gold-plated molybdenum.

Each counter had a potentially active diameter of 10 in., but this diameter was deliberately reduced to 5 in. for PC1 by covering the anode plane beyond that active circle with Mylar foils. PC1 thereby effectively collimated the incident beam in conjunction with counter 4 (see Fig. 6).

F. Logic and Timing

The details of the logic are presented in Fig. 3, while the relative timing of the various logic pulses is displayed in Fig. 4.

The over-riding concern in designing the logic was to minimize the fraction of decay positrons originating from sources other than the gas within the rf cavity. The obvious source of such backgrounds are muons stopping either in the end windows of the pressure vessel or in the walls of the rf cavity. Stops in the end windows were successfully suppressed, as mentioned in Sec. II, by adding proportional counters *inside* the pressure vessel.

Before each beam burst from the cyclotron, a pulse was sent to the logic, where it opened an approximately 0.8-msec-long gate B ("beam gate") well covering the beam spill (0.5 msec). The exact repetition rate of these pulses depended on actual cyclotron tuning, but was approximately 1000/sec.

In addition to entering the stop signature μ, the beam gate was also used to generate "rf off" and "rf on" pulses (see circuit N in Fig. 3). Both pulses were used for data routing, and the "rf on" pulse was also used for actuating a microwave switch (PIN modulator) between the klystron and the cavity (see Fig. 5).

Three fast signatures were formed with the six scintillation counters, defining muon stops (μ), and forward (e_F) as well as backward (e_B) positrons. A muon stop in the target, $\mu = (234\bar{B}5)$ opened a 5-μsec gate G, and thus defined logical time $t = 0$ (see the second line in Fig. 4). The for-

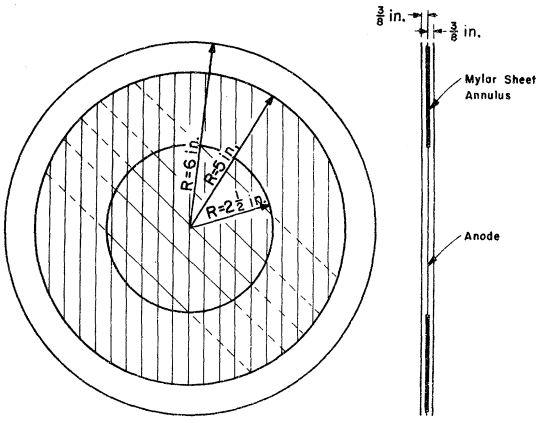

FIG. 6. Schematic drawing of planar proportional counters. Mylar annulus inserted to reduce active area to 5 in. diam are used only in PC1 (Fig. 2).

ward positron signature $e_F = [(56\bar{3})_\Delta, G]$ was formed in two steps. First a pre-e_F was defined as $(56\bar{3})$, and this was then delayed by $\Delta(0.5\ \mu\text{sec})$ before forming a coincidence with G. Since the time interval between e_F (and e_B) and μ was measured, this two-step logic allowed a measurement of the accidental background from events with $t < 0$.

The same two-step process was used in the e_B telescope. Special precautions had to be taken, however, to distinguish a backward positron from a second muon stop falling within G. The full backward-positron signature was $e_B = [(\bar{1}23\bar{5}\bar{\mu})_\Delta, G]$. Beam particles were distinguished from the backward decays in two ways. (a) Integral pulse-height selection of the output of counter 4, by setting its discriminator to fire on the large pulses produced by slow muons, and not on the smaller ones from fast positrons. The fact that 4 enters only in the μ-stop coincidence, made adding the $\bar{\mu}$ requirement equivalent to having $\bar{4}$ in e_B. The discrimination level of 4 was set by maximizing the sum of e_B and e_F, since too high a level would suppress muon stops, decreasing all e's, and a low one would excessively veto e_B's. (b) Counter 1, separated from the target by lead and aluminum beam collimators (see Fig. 2), was used as an additional veto in e_B. Positioned at 3 ft from the target, it subtended only a small solid angle for backward positrons; hence $\bar{1}$ decreased the true e_B rate by only 10%, while it cut the accidentals by a factor of 2.

The digitron,[12] a digital interval timer started and stopped by logic pulses, was used extensively in this experiment. In principle (although not in practice), the digitron was started on μ's and stopped on $e_F(e_B)$'s, and its output—the time spectra of muon decays—was stored digitally in pulse-height analyzer (PHA) memory, the channel number corresponding to the interval between digitron input pulses. If a stop pulse did not arrive within 5 μsec after a start pulse, the digitron would automatically be reset without an event being stored. It would also be reset if two start or two stop pulses arrived within 10 μsec of each other. This feature helped to insure a flat accidental background under the data.[12]

Actually, four spectra corresponding to the e_F/e_B, rf on/rf off categories were stored in four banks of 100 PHA channels. Logic pulses from a "data router" channelled each event into its proper bank and incremented an appropriate scaler when a "stored" pulse was returned from the digitron. After each run, the memory was dumped onto magnetic tape for subsequent analysis.

Actually using start and stop pulses as just indicated, an experiment completely equivalent to the previous ones[1] would have been performed. It would have had only the advantage of using time distributions rather than the integrated counts available from the scalers, but it still would have been plagued with background arising from muon stops in the pressure vessel windows. These, as was mentioned earlier, were suppressed by means of two proportional counters (PC's) within the gas.

As positrons and muons yielded somewhat overlapping pulse-height spectra, the discrimination levels at the output of the PC's had to be carefully chosen. Test muons were defined through the signature $\mu' = (2345\bar{6})$, i.e., they were mainly muon stops in counter 5. Test electrons were produced by stopping all the muons in material placed upstream of counter 2, and requiring the signature $e' = (134^*57)$, viz a complete traversal of the system (4* means 4 with an appropriately lower discriminator setting). A multichannel analyzer (PHA) gated by the signatures μ' or e' was then used to record pulse-height spectra of the test muons and positrons vs discriminator settings (see Fig. 7). The discriminated PC pulses could be added to either of the signatures to measure efficiencies vs discriminator levels; these effi-

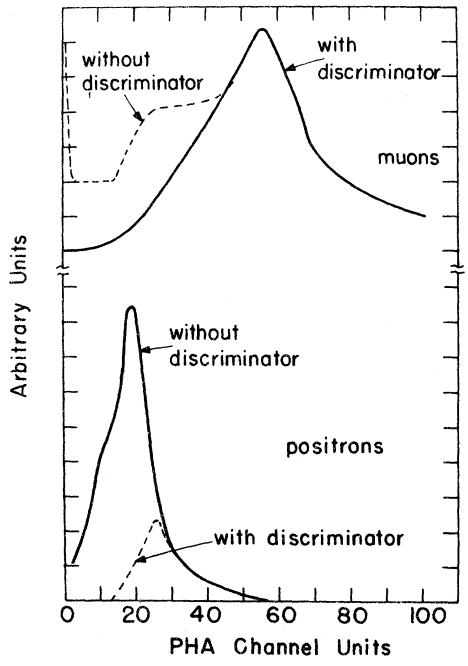

FIG. 7. Typical PC pulse spectra vs PHA channel number. The upper curves show the PC pulse height from muon stopping in the first downstream scintillator counter. Without a discriminator, positrons are clearly seen around channel 20 while the muon distribution peaks around channel 57. The discriminator clearly eliminates the smaller pulses. The lower curves with only positrons present, shows the decrease of the positrons with the discriminator requirement. The vertical scales for the muons and positrons are not the same.

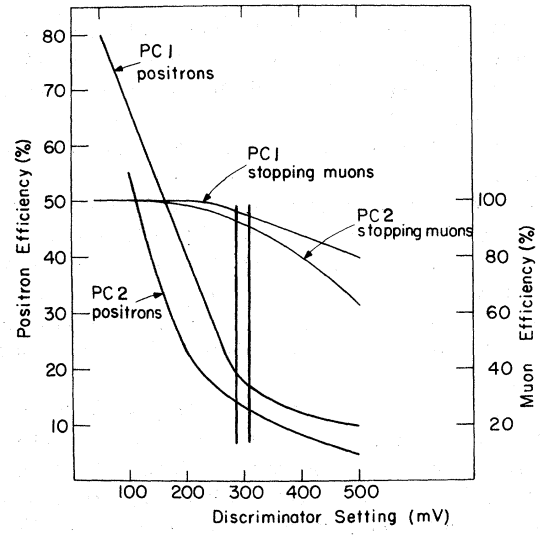

FIG. 8. Positron and muon efficiencies vs discriminator setting. Bottom scale is common to the discriminator of either PC1 or PC2. Vertical lines indicate range of typical settings under actual running conditions.

ciencies were defined as $(\mu', PC)/\mu'$ and $(e', PC)/e'$. They served to set the proper thresholds indicated by vertical lines in Fig. 8. The muon discrimination in both counters was about 90% efficient; this leads to a loss of ~10% of superstops (through the inefficiency of PC1), and a ~10% probability of retaining stops in the downstream Al window (because of PC2 inefficiency). As the decay positrons from these window stops are favored in solid angle in e_F, this explains the lower forward signals observed. The residual positron efficiency, about 15%, of the two counters leads in e_F to an equivalent loss and in e_B only to increased accidentals. Any possible dependence of these effects on the "age" of the muon decay will be discussed later.

The use of these proportional counters presented certain technical difficulties. The amplified differentiated proportional counter pulses had a slow and variable risetime (typically 1 μsec) with a wide and variable pulsewidth (typically 5 μsec) compared with the standard pulses from the "fast" logic. Matching to the latter was achieved by shaping the PC pulses, through discriminators (set to fire on the larger muon pulses, rather than the smaller positron pulses) and setting the discriminator pulsewidths ($\geq$10 μsec) much larger than those of the inputs (see Fig. 4), thus eliminating the effects of the jitter in pulsewidth and timing.

A *superstop* coincidence $S \equiv [(\mu)_\Delta, \text{PC1}, \overline{\text{PC2}}]$ was formed by delaying the μ by 5 μsec, an overly sufficient time for the PC's to fire, and then allowing this delayed signature to make coincidence with the PC's. Hence 5 μsec after a μ, the superstop indicated whether or not the stop had occurred in the volume of interest. A *superpositron* was defined as an e_F or e_B accepted by the digitron stopped on superstops.

Our usual running mode was to start the digitron on e's and to stop it on S's, relying upon the digitron to reset itself if no superstop occurred.

IV. AUXILIARY MEASUREMENTS

A. Beam Polarization and Range Determinations

The muon channel[13] at the Fermi Synchrocyclotron provided muons from π decays along its length. A bending magnet at the end of the channel momentum selected the particles and directed them into our target.

A beam of longitudinally polarized muons is obtained from a pion beam by selecting those muons which originate from approximately backward (forward) pion decays in the pion rest frame. These muons have lower (higher) momenta than the parent pions and are polarized parallel (antiparallel) to their momenta.

The degree of polarization of both forward and backward muons was determined by comparing the relative forward decay positron rates of muons stopped in Al and S targets of equal stopping power; Al does not depolarize and S does. The backward beam was $(55 \pm 5)\%$ polarized and the forward 70%. Since the signal height is directly proportional to the initial polarization P_0 the latter is a very important consideration in the experimental design, though not the only one.

The relative amount of beam stopping in the argon gas depends upon the range spread of the beam. The full width half-maximum (FWHM) of the backward beam measured with the probe counter (see Fig. 9 and Sec. II B) was 1 g/cm^2, while the forward beam yields ~2.5 g/cm^2. Also the backward

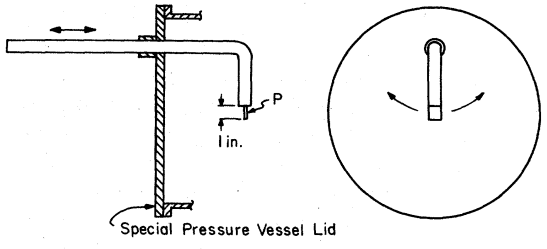

FIG. 9. Narrow probe counter 1 in. $\times \frac{1}{2}$ in. $\times$1 mm is mounted on the end of a curved light pipe which extends through a special pressure vessel lid. The lid has a seal which allows the counter unit to be moved both longitudinally and rotated. This freedom of movement allowed complete mapping of the beam distribution.

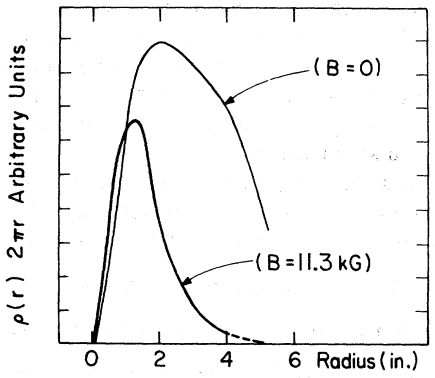

FIG. 10. Preliminary stopping muon distribution. Styrofoam and the pressure-vessel Al dome windows were used to simulate target conditions. The "focusing" effect of the magnetic field is clearly shown.

beam, having a momentum around 75 MeV/c, is not contaminated with π's as is the forward one. Finally, the lower traversal rates per muon stop result from the backward beam, leading to a smaller percentage of accidentals. For these reasons, we decided to accept the lower polarization and to use the backward beam.

B. Probe Counter and Beam Mapping

The muon-stop distribution $\rho(\vec{r})$ in the gas was needed for the detailed calculation of the static and rf field averages and of the Lorentzian signal height (see Sec. II).

Some preliminary measurements of the muon-stop density $\rho(\vec{r})$ in the midplane ($z = 0$) of the magnet were made by means of the "self-positrons" discussed below using realistic collimation, the actual Al end windows, and styrofoam blocks to stimulate the Ar gas. The results are shown in Fig. 10. These curves, taken at the peak of the muon range curve, show clearly the "focusing" action of the magnetic field.

To determine $\rho(\vec{r})$ accurately, a small probe counter (P) consisting of a 1×0.5-in.^{2} scintillator 1 mm thick was inserted through the downstream end of the pressure vessel (see Fig. 9) so that it was capable of longitudinal motion (parallel to the cylindrical axis of the pressure vessel) and rotational motion (sweeping perpendicular to the cylinder axis). Counters 6 and 7, normally in the e_F signature, were not inserted, and the downstream Al window was replaced by a special plate.

For these measurements, the μ signature which opens the gate G was defined as $\mu' = (345P)$. "Self-positrons," i.e., positrons from muon decays in P, were defined as (G, P); they measured a quantity proportional to $\rho(\vec{r})$ directly. The coincidence $e'_B = [(G, P), 3, 4]$ was hence directly proportional to $\rho(\vec{r})$ times the solid angle $\Omega(\vec{r})$ of the backwards telescope (for most purposes, in view of the symmetry of the apparatus, this is identical to that of the forward telescope).

The beam was mapped at the two operating pressures, viz, 5 and 18 atm. Figures 11 and 12 illustrate the results at 18 atm, for the vertical midplane of the cavity. As Fig. 12 shows, the horizontal (x) and vertical (y) beam profiles had within 0.125 in. the same FWHM (~3.5 in.), i.e., considerably less than the cavity radius (this justifies the 90% radius of the stop distribution indicated in Fig. 2).

Scans similar to those illustrated were also made at $z = \pm 4$ in. (1 in. from the cavity ends). They showed very little departure from the results in the midplane; the crosses in Fig. 12(a) represent the observed axial variations in peak height. Variations in width were absent within statistics.

The profiles measured at 5 atm were entirely similar, except for a slight increase (0.25 in.) in width.

The slight vertical displacement (by 0.5 in.) of the beam direction from the cavity axis visible in Fig. 12(b) is of no practical consequence.

The probe counter, introduced *radially* into the midplane of the pressure vessel, was also used to obtain the range curves (Figs. 12 and 14) already discussed in Sec. IV A. Note that the "window" of this range curve is constituted by the thickness of the probe, i.e., 0.1 cm $\simeq$ 0.1 g/cm^2 of $(CH_2)_n$

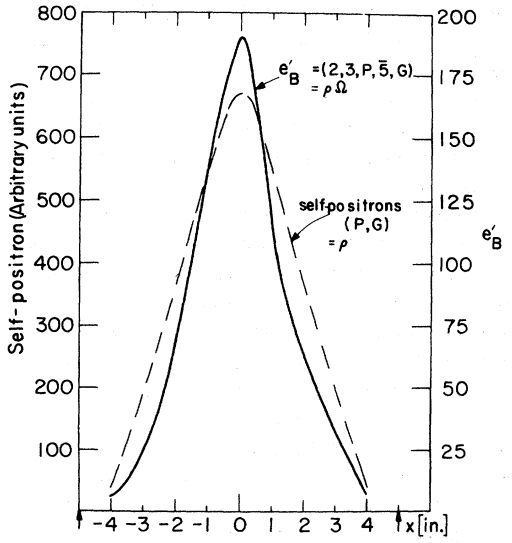

FIG. 11. Distributions of ρ (self-electrons) and $\rho\Omega$ ("eb") at $y = z = 0$, i.e., central horizontal scans in the midplane of the cavity in Ar at 18 atm. Note that the curve for ρ is identical with the top curve in Fig. 12. Arrows indicate cavity radius.

equivalent to 0.15 g/cm^2 of argon. In this configuration, the approximate symmetry of $\rho\Omega$ in the two electron telescopes was verified.

C. rf Measurements

The microwave equipment is shown in Fig. 5. The frequency was continuously monitored with a Hewlett-Packard HP5254 scaler and was maintained constant to within 0.15 ppm.

Using the considerations of Sec. II to choose the value of the effective microwave field B_1 and the measured Q of 40 000, the rf power in the cavity was chosen to be about 70 W. The power level was set for each frequency by measuring the forward and the reflected power. The reproducibility of a given setting was about 1%.

During actual data taking the reflected power and the cavity power (measured with a pickup loop located 135° from the rf drive loop) were monitored continuously, while the forward power was checked about every hour.

V. DATA ACQUISITION

For each rf frequency ω_i a data run consisted of recording the four decay time distributions (digitron spectra) in the PHA memory and dumping the memory onto magnetic tape at the end of each run. The contents of the PHA memory could, of course, be analog displayed on a scope in the usual manner,

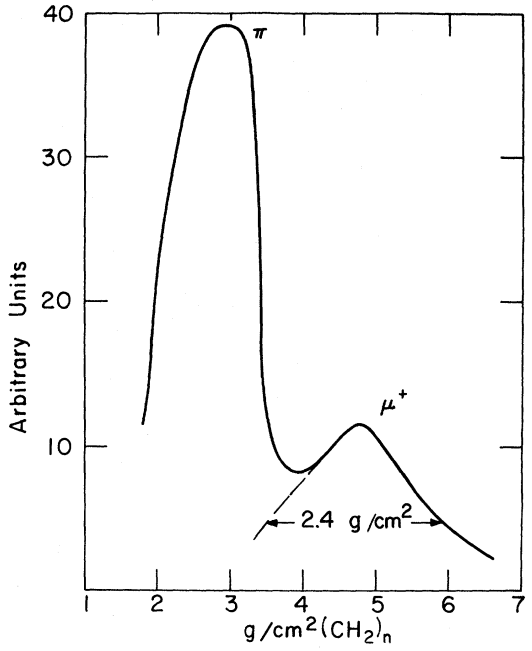

FIG. 13. Forward-beam range curve taken in 1-mm-thick scintillator. Notice width of the μ peak and the obvious contamination of the μ's by the π's.

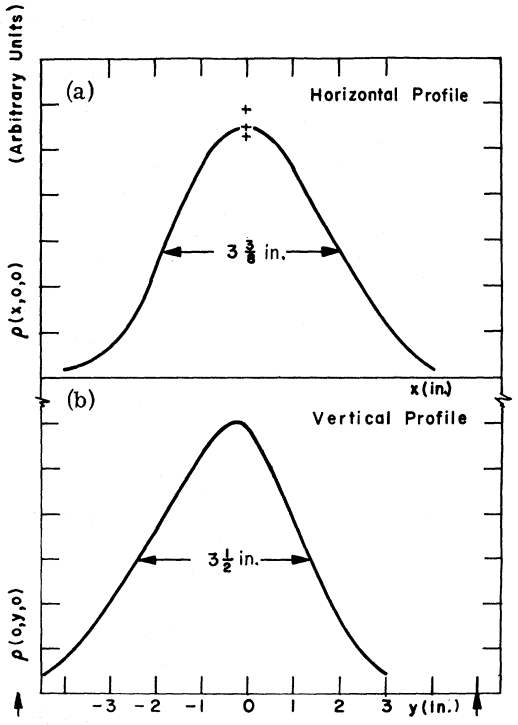

FIG. 12. Beam profiles $\rho(\vec{r})$ in the vertical midplane ($z=0$) of the cavity, measured in Ar at 18 atm. Vertical axis is denoted y, horizontal x. The crosses near the top of the curve (a) indicate variations as a function of z. Arrows indicate cavity radius.

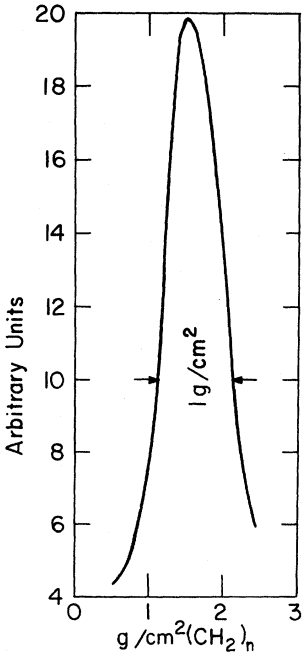

FIG. 14. Backward-beam range curve taken in 1-mm-thick scintillator, allowing its narrow energy spread to be clearly seen.

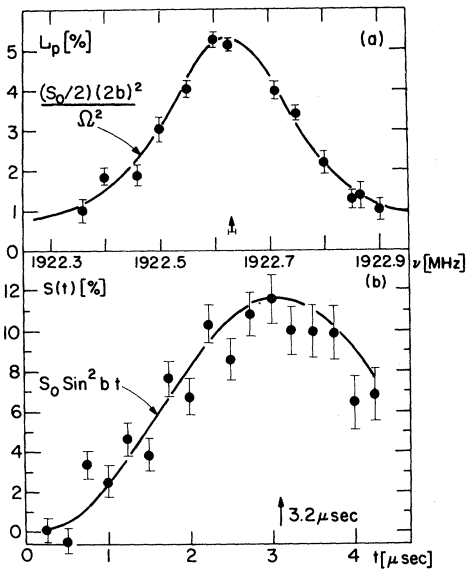

FIG. 15. Typical data with fitted curves. The error bars (1 standard deviation) represent counting statistics. (a) Fit to the pseudo-Lorenztian L_p, with the data points shown. (b) Fit to one of a set of time-dependent curves $S(t)$ corresponding to the central point (1922.632 MHz) on the curve in (a).

or printed out on paper tape. Runs were taken alternatively with frequencies ω_i above and below the expected peak ω_0 of the Lorentzian resonance to minimize the effects of potential changes in running conditions. During each run, the beam rate, the stops μ, the superstops S, and all four categories of both "ordinary" positrons and "superpositrons" were recorded on scalers. Also, as described in Sec. III, the rf oscillator frequency, cavity power, and the reflected power were continuously monitored.

While the final results were obtained by computer analysis of the magnetic tapes, the "superpositron" scaler information was sufficient (together with PHA printouts giving the accidental levels from $t<0$ channels) to obtain preliminary Lorentzian resonance curves during actual data taking. This could help to detect any serious changes while running; none were observed.

Rates

When the cyclotron was operating normally, the beam monitor (counter 1) rate was 1.5×10^4/sec, and the corresponding superstop rate was 10^3/sec at high pressure and 350/sec at low pressure.

The ratio of superstops to ordinary stops was about 48% in the high-pressure runs, and about 22% at low pressure. The total yield of all superelectrons per superstop was 23%, while the measured accidental background equaled 4% forward and 8% backward. For a standard datum point about 2×10^5 superpositrons of each category were collected. Under normal beam conditions, each high-pressure point took about 1 h, so that the data for a resonance curve such as shown in Fig. 15 could be obtained in 24 h.

In the course of the experiment, there were difficulties in cyclotron operation and the muon beam rate was often below "normal." These cyclotron problems affected, however, only the beam rate and not the duty cycle or other beam parameters. Hence, their sole effect other than protracting the data-taking time was to reduce the level of accidental background.

VI. DATA ANALYSIS

The input data for the resonances were the decay positron time distributions (digitron time spectra). A set of four such spectra, representing backward and forward decays with rf on/rf off, were recorded simultaneously at a set of frequencies ω_i centered about the anticipated resonance frequency ω_0. These spectra $N(\omega_i, t_k)$ were stored in four 100-channel banks of a 400-channel PHA memory. The digitron clock (see Sec. III) was set for 50 nsec/channel, so that each bank covered 5 μsec; 4.5 μsec of these (~ two muon lifetimes) were allocated to the actual decay spectra, while 0.5 μsec of "negative time" served to monitor accidental background.

This individually measured accidental background A_m may, if assumed flat, be subtracted bin by bin from the data in a given bank. If the background is small and equal for the rf-on and rf-off data, it is legitimate to subtract it from only the normalizing denominator of the signal [N_{off} in Eq. (10)] and not from its numerator ($N_{off}-N_{on}$). As A_m was small in the present experiment (~ 4% forward and ~ 8% backward), this approach was the one adopted. We had, however, to make sure that the actual background ($t>0$) was indeed flat and equal to A_m. To check this, rf-off data were fitted to $N_{off}(t)=N_0e^{-\lambda t}+A$, ($1/\lambda=2.20$ μsec = muon lifetime), and A was compared to A_m.

The expectation $A_m=A$ was indeed reasonably well confirmed for e_B data, but not for e_F data. For the latter, the χ^2 was large and A was about four times A_m. As discussed briefly in Sec. II, we attribute this effect to the fact that PC2 can, with about 15% probability, fire on an e_F and thus "self-veto" a good event, and that the probability for this vetoing to occur is not constant over the lifetime of each muon: In fact, the slow PC rise time makes the probability of self-vetoing approach zero for late decays. This hypothesis means that for e_F, the poor χ^2 corresponds not to a larger flat accidental background, but to a distortion of $N(t)$. It was confirmed by the fact that data taken without

PC2 gave agreement between A and A_m and good χ^2 fits. Hence A may be subtracted as the correct background, but $N_{off}(t)$ in Eq. (8) and $N_{on}(t)$ in Eq. (9), should be multiplied by some efficiency factor $g(t)$, which may differ for the forward and the backward telescopes. Three different methods were used to extract the resonance frequency for given running conditions (e. g., argon density, rf power, etc.). These will be discussed now; two of them are explicitly independent of $g(t)$.

A. Time-Dependent Signal

This method is both the most straightforward one and has the greatest statistical power. Its only drawback is that it is less familiar than the methods which fit to Lorentzians.

In this method, the data is fitted directly to Eq. (12). The fitted parameters were b^2, S_0, and ω_0, with all three parameters common to all data. The statistical error on each point was $[2/N_{off}(\omega_i, t_k)]^{1/2}$. In one modification the rf power ($\propto b^2$) was fitted individually to each run ω_i to cross check the consistency of the rf power taken at fixed running conditions. This resulted in almost no change in the fitted center frequencies nor in the value of χ^2.

In this particular method there are no problems with $g(t)$, since by Eq. (10), any such common factor divides out.

B. Lorentzian

In this method, the same three parameters were fitted to Eq. (13), with the data for each point ω_i being simply the sums of the individual time spectra:

$$N^L_{off}(\omega_i) = \sum_k N_{off}(\omega_i, t_k) ,$$

$$N^L_{on}(\omega_i) = \sum_k N_{on}(\omega_i, t_k) ,$$

and the data points for L become

$$L(\omega_i) = \{[\sum_k N_{off}(\omega_i, t_k) - \sum_k N_{on}(\omega_i, t_k)]/ \sum_k N_{off}(\omega_i, t_k)\} ,$$

where any factors $g(t)$, though not expected to produce any change in the center frequency, cannot clearly be excluded from such effects either. The error of each point ω_i is $(2/N^L_{off})^{1/2}$.

C. Pseudo-Lorentzian

To form a Lorentzian-type signal which is explicitly independent of $g(t)$, the data points were formed as follows:

$$L_p(\omega_i) = \sum_k \frac{[N_{off}(\omega_i, t_k) - N_{on}(\omega_i, t_k)]}{N_{off}(\omega_i, t_k)} .$$

The justification for fitting this signal to a Lorentzian form may be seen by integrating the signal $S(t)$, Eq. (12), over the observation time T (again suppressing the subscripts av and eff):

$$L_p(\omega_i) = \frac{1}{T}\int_0^T S\, dt = \int_0^T \tfrac{1}{2}S_0\left(\frac{2b}{\Omega}\right)^2 [1 - \cos(\Omega T)]\, dt$$

$$= \frac{\frac{1}{2}S_0(2b)^2}{[(2b)^2 + \Delta\omega^2]}\left(1 - \frac{\sin(\Omega T)}{\Omega T}\right)$$

$$= \frac{H(\frac{1}{2}\Gamma)^2}{(\frac{1}{2}\Gamma)^2 + (\Delta\omega)^2}\left(1 - \frac{\sin(\Omega T)}{\Omega T}\right) ,$$

which yields a Lorentzian times a correction factor $[1 - \sin(\Omega T)/\Omega T]$ which is symmetric about ω_0. For our rf power $\{\Omega = [(2b)^2 + \Delta\omega^2]^{1/2} = [(10^6)^2 + \Delta\omega^2]^{1/2}\}$ and observation time T, directly calculating this correction term produces a maximum of 20% difference in L_p, over our experiment frequency range ω_i. Considering this variation about a mean $\langle L_p\rangle_{av}$ as $\pm 10\%$, a value comparable or less than the statistical errors of each experimental point ω_i, $\langle L_p\rangle_{av} \approx L_p$ can be expected to yield reasonable fits.

The error of each datum point ω_i in L_p is formed quite differently from the preceding cases, namely,

$$\sigma(\omega_i) = [\sum_k \sigma^2(\omega_i, t_k)]^{1/2} = [\sum_k 2/N_{off}(\omega_i, t_k)]^{1/2} .$$

In this case, the error on each point ω_i increases with increasing observation time T.

1. Statistical Considerations

The statistical error in determining ω_0 from fits to a given functional form $F(X)$ may be calculated as

$$\frac{1}{\sigma^2(\omega_0)} = \sum \left(\frac{\partial F}{\partial \omega_0}\right)^2 \Big/ \sigma^2 = \sum_i \left(\frac{\partial F(X_i)}{\partial \omega_0}\right)^2 \Big/ \sigma^2(X_i) .$$

For the general Lorentzian form $H(\frac{1}{2}\Gamma)^2/[(\frac{1}{2}\Gamma)^2 + \Delta\omega]$ and assuming an integration over ω from $-\infty$ to $+\infty$, we find $\sigma(\omega_0) = 2(\frac{1}{2}\Gamma)\sigma(\omega_i)/[H\pi^{1/2}]$, where $\sigma(\omega_i)$ is the statistical accuracy, assumed constant, of each datum point ω_i. For the Lorentzian fit, Eq. (13), $H = \frac{1}{2}S_0(\Gamma_{rad}/\Gamma)^2$ and $\Gamma^2 = \Gamma^2_{rad} + \Gamma^2_0 = (2b)^2 + \lambda^2$, while for the pseudo-Lorentzian, ignoring the correction term, $H = \frac{1}{2}S_0$ and $\Gamma = \Gamma_{rad} = 2b$. The ratio of these statistical weights becomes

$$\frac{\sigma_{L_p}(\omega_0)}{\sigma_L(\omega_0)} = \frac{\Gamma_{L_p}}{\Gamma_L}\frac{H_L}{H_{L_p}}\frac{\sigma_{L_p}(\omega_i)}{\sigma_L(\omega_i)}$$

$$= \left(\frac{\Gamma_{rad}}{\Gamma}\right)^3 \frac{\sigma_{L_p}(\omega_i)}{\sigma_L(\omega_i)}$$

$$= \left[1 + \left(\frac{\lambda}{2b}\right)^2\right]^{-3/2} \frac{\sigma_{L_p}(\omega_i)}{\sigma_L(\omega_i)} .$$

The computation for $\sigma_{TDC}(\omega_0)$ for S is less straightforward. First rewrite Eq. (12) as $S = L_p[1 - \cos\Omega t]$, where $L_p = (S_0/2)(2b)^2/\Omega^2$ is the pseudo-Lorentzian. Then

$$\frac{\partial S}{\partial \omega_0} = L_p\Omega \sin(\Omega t) + L'_p(1 - \cos\Omega t) ,$$

where the

$$L'_p = \frac{\partial L_p}{\partial \omega_0} = \frac{2H(\frac{1}{2}\Gamma)^2\Delta\omega}{\Omega^2} .$$

TABLE I. Results of analysis using various functional forms on run 1.

Type	e_B ν_0	e_B FWHM	e_B $[\chi^2/D]^{1/2}$	e_F ν_0	e_F FWHM	e_F $[\chi^2/D]^{1/2}$	e_{sum} ν_0	e_{sum} FWHM	e_{sum} $[\chi^2/D]^{1/2}$
				No background corrections					
L	631.1±11.9	401±55	1.6	621.3±12.3	431±59	1.3	621.5±7.6	413±35	1.3
L_p	627.4±7.7	312±31	1.4	634.4±7.8	386±34	0.99	630.3±5.4	322±22	1.18
TDC	634.0±5.0	397±7	1.14	639.5±5.6	390±8	1.19	636.4±4.0	394±5	1.21
TDC All powers fitted	636.7±5.8	...	1.19	632.5±5.3	...	1.14	634.7±4.1	...	1.2
				With flat-background corrections					
L	430.3±11.0	430±44	1.28	620.3±11	409±43	1.2	627.1±7.9	422±32	1.27
L_p	631.4±7.9	362±29	1.08	630.1±7.6	388±28	1.02	631.1±6.2	352±23	1.19
TDC	633.0±5.0	388±8	1.21	639.5±5.7	388±7	0.99	636.1±4.0	388±7	1.18

Note that for all values of ω_i, $L_p\Omega > L_p'$ and henceforth we will assume the second term approximately equals 0. Then

$$1/\sigma_{\mathrm{TDC}}(\omega_i)^2 = \sum_i \sum_k N_0 L_p^2 \Omega_i^2 \sin^2(\Omega_i t_k) e^{-\lambda t_k},$$

where the exponential $(N_0 e^{-\lambda t_k})$ comes from $1/\sigma^2(\omega, t_k)$. The sum over time produces

$$1/\sigma_{\mathrm{TDC}}^2(\omega_0) = \tfrac{1}{2}(\tfrac{1}{2}\Gamma)^2 \sum_i L_p^2(\omega_i) F N_0,$$

where

$$F = \left(\frac{\Gamma}{2\lambda}\right)^3 - \frac{(2\lambda/\Gamma)^3 + (2\lambda/\Gamma)(4\Omega/\Gamma)^2 + 8(2\Omega/\Gamma)^3}{[2\lambda/\Gamma + (4\Omega/\Gamma)^2]^3}.$$

Notice that the first factor in F is frequency independent while the second one varies, for our rf power, from 0.08 to 0. Now summing the frequencies, assuming F is frequency independent, produces

$$\sigma_{\mathrm{TDC}}^2 = \frac{8(\frac{1}{2}\Gamma)^2}{[N_0 \pi \tfrac{1}{2} S_0] F} \approx \frac{8(\frac{1}{2}\Gamma)^2 (2\lambda/\Gamma)^3}{(N_0 \pi \tfrac{1}{2} S_0)}.$$

The demonstration that the statistical power of this fit increases with rf power should be considered more carefully. The derivation begins with an assumption that all the effects of the rf power present may be replaced by a suitable average (see Sec. II). The assumption may well fail at high rf powers.

The results of the various fitting procedures are shown for our data in Tables I–III with the statistical errors expanded by $R = [\chi^2/D]^{1/2}$, where D is the number of degrees of freedom. The cases with and without a flat background subtraction, based on the measured background, are shown.

VII. RESULTS AND CONCLUSIONS

Our experimental results, obtained by analyzing the data in terms of a time-dependent signal (method of Sec. V A) are (a) run 1[14]: $\nu_1(1.26\times10^4$ Torr) = 1922.6347(41) MHz (2.15 ppm); (b) run 2: $\nu_1(3.15\times10^3$ Torr) = 1922.7250(46) MHz (2.4 ppm); (c) run 3: $\nu_1(1.26\times10^4$ Torr) = 1922.6263(32) MHz (1.7 ppm), where the pressures in brackets have been corrected to 0 °C, but not for departure from the ideal-gas law. The errors are mainly statistical, but include density and systematic errors.

The errors, due to variations in rf-power level was estimated by taking the Lorentzian data points, assuming that each point suffered a ±1% Gaussian

TABLE II. Results of analysis using various functional forms on run 2.

Type	e_B ν_0	e_B FWHM	e_B $[\chi^2/D]^{1/2}$	e_F ν_0	e_F FWHM	e_F $[\chi^2/D]^{1/2}$	e_{sum} ν_0	e_{sum} FWHM	e_{sum} $[\chi^2/D]^{1/2}$
				No background corrections					
L	717.7±11.6	307±38	1.19	742.5±8.8	300±9	1.03	730.5±7.2	303±24	1.12
L_p	719.8±8.5	256±26	1.33	738.1±8.0	282±20	1.21	729.4±4.9	252±15	1.06
TDC	718.9±6.5	271±12	1.07	733.7±6.0	296±10	1.01	726±4.5	285±8	1.05
				With flat-background corrections					
L	716.4±13.4	328±45	1.13	746.5±10.8	316±37	0.74	732.0±8.3	323±28	1.03
L_p	720.3±9.0	266±28	1.17	742.8±8.1	278±27	0.71	731.2±5.5	271±18	0.89
TDC	718.4±6.6	284±6	0.97	732.3±6.6	269±8	1.14	725.0±4.6	277±7	1.06

TABLE III. Results of analysis using various functional forms on run 3.

Type	e_B ν_0	e_B FWHM	e_B $[\chi^2/D]^{1/2}$	e_F ν_0	e_F FWHM	e_F $[\chi^2/D]^{1/2}$	e_{sum} ν_0	e_{sum} FWHM	e_{sum} $[\chi^2/D]^{1/2}$
				No background corrections					
L	636.1±6.88	339±21	1.09	620.5±13	374±46	1.6	629.1±6.2	357±18	1.2
L_p	632.3±5.1	275±15	1.09	625.6±8.7	303±29	1.26	629.2±4.1	287±13	1.03
TDC	625.4±4.3	344±6.6	1.04	623.0±5.2	349±7.7	1.15	625.6±3.3	346±5	1.12
TDC All powers fitted	626.9±4.5	...	1.04	623.1±5.5	...	1.12	626.3±3.3	...	1.04
				With flat-background corrections					
L	635.0±7.15	345±24	1.04	619.2±13.6	345±47	1.04	627.8±6.4	364±22	1.16
L_p	631.0±5.48	277±17	1.05	625.3±8.8	302±27	1.38	628.8±4.4	289±14	1.2
TDC	628.1±4.3	333±6	1.08	623.4±5.3	346±7	0.99	626.3±3.2	338±4.7	1.00

variation in rf power. A new Lorentzian fit to the data "corrected" for these simulated variations was made. The change in the resultant center frequency corresponds to the error estimate in Table IV. All of the errors are listed in Table V. The average of runs 1 and 3, $\Delta\nu(1.26\times10^4$ Torr) = 1922.6295 (45) MHz and (b) yield, by *linear* extrapolation,

$$\nu_1(0\ \text{Torr}) = 1922.7569\,(78)\ \text{MHz}\quad (4.06\ \text{ppm}) \tag{14}$$

and a fractional pressure shift (FPS)

$$\frac{1}{\nu_1}\frac{\partial\nu_1}{\partial P} = -5.27\,(40)\times10^{-9}/\text{Torr}. \tag{15}$$

Frequency (14) in turn corresponds to

$$\Delta\nu(0) = 4463.317\,(18)\quad (4.06\ \text{ppm}) \tag{16}$$

using the value of $g'_\mu/g_e = 0.004\,836\,26$ available at the time of the conclusion of the present experiment[10] and applying a 3.1 kHz correction for departure from the "magic" field.

Note that first extrapolating $\nu_1(p)$ to zero density and then using Eq. (4) to get $\Delta\nu(0)$ automatically allows for a pressure shift of g_j. The relevant quantity is g_j/g'_μ, and even at a fixed pressure, the influence of such a g_j shift would be probably negligible compared to the current uncertainty in g'_μ (~4 ppm). In Kr at 15 atm the g_j shift is of the order of 10 ppm,[9] and theoretical arguments[15] imply that it should be about ten times smaller in Ar.

Using the current value, $g'_\mu/g_e = 0.004\,836\,29$, based on a new determination of f_μ/f_p[16] and on a recent muonium work in this laboratory,[9] one obtains

$$\Delta\nu(0) = 4463.313\,(18)\ \text{MHz}\quad (4.06\ \text{ppm}). \tag{17}$$

This result is in clear disagreement with the Yale results mentioned in the Introduction, viz.

$$\Delta\nu(0) = 4463.15\,(06)\ \text{MHz}\quad (13\ \text{ppm})$$

(Ar, high field[3]),

$$\Delta\nu(0) = 4463.220\,(20)\ \text{MHz}\quad (4.5\ \text{ppm})$$

(Ar, low field[5]),

and

$$\Delta\nu(0) = 4463.262\,(12)\ \text{MHz}\quad (2.7\ \text{ppm})$$

(Kr, low field[5]),

but was confirmed by subsequent work in this laboratory.[9]

Similarly, the low-pressure point may be used in conjunction with the "atomic" FPS[17] of $(-4.78\pm0.03)\times10^{-9}$/Torr to produce

$$\Delta\nu(0) = 4463.307\,(14)\ \text{kHz}\quad (3\ \text{ppm})$$

in good agreement with Eq. (17). These results are plotted in Fig. 16, where some of the lower-pressure Yale results have also been included.

The disagreement between our results and those of the Yale group is not confined to the extrapolated $\Delta\nu(0)$ but includes also the magnitude of the FPS. Equation (15) is closer to the value $-4.78\,(3)\times10^{-9}$

TABLE IV. Data from final flat-background time-dependent fits and statistical errors; worst error from Lorentzian fits. [Errors are statistical only. These fitted errors were increased by factor $[\chi^2/D]^{1/2}$ when this is >1. Errors do not include 2.5-kHz pressure measurement errors at high pressures nor 1-kHz systematic power errors. These are included in the final errors presented: high pressure 1922 629.5 (4.5); low pressure 1922 725 (5.7).]

Run number	Pressure (Torr 0 °C)	ν_0	$[\chi^2/D]^{1/2}$	Worst error
1	1.26×10^4	634.7±4.1	1.2	9.3
2	3.15×10^3	725.0±4.6	1.06	7.2
3	1.26×10^4	626.3±3.2	1.0	6.4

TABLE V. Summary of errors in determination of $\Delta\nu(0)$.

		Absolute (kHz)	Relative (ppm)
1(a)	Statistical error in ν_1 (1.26×10^4 Torr)	2.5	1.3
1(b)	Statistical error in ν_1 (3.15×10^3 Torr)	4.5	2.34
2(a)	Pressure error in ν_1 (1.26×10^4 Torr)	2.5	1.30
2(b)	Pressure error in ν_1 (3.15×10^3 Torr)	1.0	0.52
3	Systematic rf-power error in each ν_1	1.0	0.52
4(a)	Final error in ν_1 (1.26×10^4 Torr)	4.5	2.34
4(b)	Final error in ν_1 (3.15×10^3 Torr)	5.6	2.91
5(a)	Error in extrapolation to $\nu_1(0)$	7.8	4.06
5(b)	5(a) converted to $\Delta\nu(0)$	18.1	4.06
6	Uncertainty in conversion from $\nu_1(0)$ to $\Delta\nu(0)$	(a) 4.5	1.01
	due to $\left\{\begin{matrix}\text{(a) 13 ppm}\\ \text{(b) 4 ppm}\end{matrix}\right\}$ uncertainty in g'_μ/g_e	(b) 1.4	0.3
7	Correction of $\Delta\nu$ for known departure from correct "magic" field value, $\Delta B = 36$ G	3.1	0.7
8	Uncertainty in field correction	0.3	0.07
9	Total error in $\Delta\nu(0)$ when determined without external knowledge of (linear) pressure shift, i.e., vector sum of 5(b), 6(b), and 8	18.16	4.07
10(a)	Error in linear extrapolation to $\nu_1(0)$ from $\nu_1(3.15\times10^3$ Torr) only, using "atomic" FPS	5.8	3.02
10(b)	10(a) converted to error in $\Delta\nu(0)$	13.5	3.02
11	Total error in $\Delta\nu(0)$ when determined using external (atomic) value of pressure shift, i.e., vector sum of 6(b), 8, and 10(b)	13.6	3.04

reported[17] for atomic H in Ar. The pressure shifts of $\Delta\nu$ for H, D, and T are accurately known[17] from experiment and supply no evidence for an isotope effect; there are also no theoretical reasons to expect one.[18]

Both discrepancies tend to confirm the suspicion[6] that the pressure shift is not purely linear over *large* ranges of pressure, but includes at least a quadratic term, viz.

$$\Delta\nu(p) = \Delta\nu(0)\,(1 + ap + bp^2 + \cdots)\,. \qquad (18)$$

The Yale Ar data in question,[5] taken at much higher pressures (≥ 30 atm) than those presented here (≤ 18 atm), should be more affected by the quadratic term than ours. With b positive, a linear fit would falsify the value of both $\Delta\nu$ and the FPS coefficient, in the sense of a reduction.[19]

To further test the idea of a nonlinear pressure shift, a fit of the available data was made to Eq. (18) with the important proviso that the linear coefficients a were constrained to their hydrogen values[17,20]

$$a_{\mathrm{Ar}} = -4.78\times10^{-9}/\mathrm{Torr}\,,$$

$$a_{\mathrm{Kr}} = -10.4\times10^{-9}/\mathrm{Torr}\,.$$

In other words, the fit was for two parameters: the intercept and the quadratic coefficient.

The Yale Ar data used in this fit were taken from

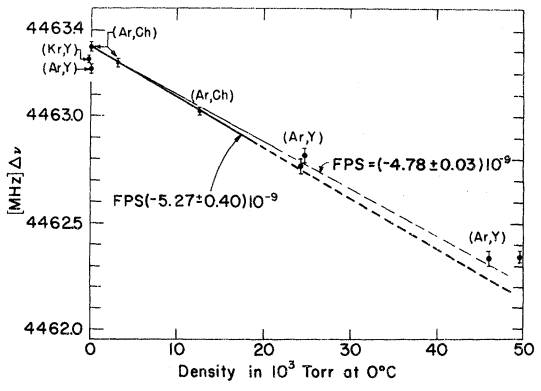

FIG. 16. Linear extrapolation of Chicago argon (Ar, Ch) data to vacuum. Yale results in Ar and Kr are labeled (Ar, Y) and (Kr, Y). The points at zero density are extrapolated intercepts. This graph differs slightly from Fig. 3 of Ref. 14 in that (a) a later (Ref. 5) Yale Kr intercept is plotted rather than that of Ref. 4; (b) the data and curve were replotted.

TABLE VI. Final values.

		TDC fit	Lorentzian fit
A	Chicago linear values	$\nu(0) = 1922.7569\ (78)$ MHz FPS $= -[5.27\ (40)] \times 10^{-9}$/Torr $\Delta\nu(0) = 4463.313\ (18)$	$\nu(0) = 1922.758\ (11)$ FPS $= -[5.28\ (60)] 10^{-9}$/Torr
		Fits to $\Delta\nu(p) = \Delta\nu(0)\ [1 + aP + bP^2]$ with "a" constrained to atomic value $\{= -[4.78(3)] \times 10^{-9}$/Torr in Ar; $[-10.4(2)] \times 10^{-9}$/Torr in Kr$\}$	
B	University of Chicago (TDC)	$\nu(0) = 4463.305\ (14)$ MHz	$b = -3.95\ (330) \times 10^{-14}$
C	Graphed Yale Ar	$\nu(0) = 4463.288\ (22)$	$b = +8.5\ (4.2) \times 10^{-15}$
D	Combined Yale/University of Chicago Ar	$\nu(0) = 4463.288\ (8)$	$b = +8.3\ (2.8) \times 10^{-15}$
E	Simulated Yale Kr	$\nu(0) = 4463.279\ (12)$	$b = +7.3\ (2.0) \times 10^{-15}$

the graph in Ref. 4 and are, of course, an approximation to the exact value. The Yale Kr points were simulated over their pressure range using the values $\Delta\nu_{Kr}$ and a_{Kr} presented in Ref. 5.

The results and statistical errors of this fit are presented in Table VI. The errors resulting from the uncertainty in a_{Kr} and a_{Ar} (about 10.5 kHz for Kr and about 2.2 kHz for Ar) are not included. While the exact values and errors must await the publication of the Yale data, the following results seem sufficiently dramatic as to be unaffected by detailed data differences. (a) The quadratic coefficient is compatible with zero in the Chicago data, indicating that indeed we were operating at a sufficiently low pressure to justify a linear extrapolation. (b) The intercepts of the Yale Ar and Kr data are in reasonable statistical agreement and the Yale data, even in their simulated form, seem to imply a quadratic coefficient with significant accuracy. Surprisingly, it seems that this quadratic coefficient is the same for both gases.

With this interpretation on the high-pressure data, all current (available before April, 1971) data on the muonium hyperfine structure frequency are in reasonable agreement.

The ratio of (17) with the hydrogen hyperfine splitting[21]

$$\frac{\Delta\nu(\mu e)}{\Delta\nu(pe)} = \frac{\mu_\mu}{\mu_p}\left(\frac{1+m_e/m_p}{1+m_e/m_\mu}\right)^3 (1+\delta_p-\delta_\mu) \qquad (19)$$

will yield a value of μ_μ/μ_p for comparison with other experiments. Here δ_μ (179 – 5 ppm) and δ_p (35 ppm) represent the relativistic recoil and finite-size corrections; various other electrodynamic corrections, identical for the two atoms, cancel in the ratio to the first order. Note that no allowance is made in (19) for the proton polarizability. With (17) and $\Delta\nu(pe) = 1420.40575$ MHz,[21] (19) yields

$$\mu_\mu/\mu_p = 3.183\,331\ (13)$$

in good agreement with a later determination in this laboratory[9] $[\mu_\mu/\mu_p = 3.183\,337\ (13)]$ and with

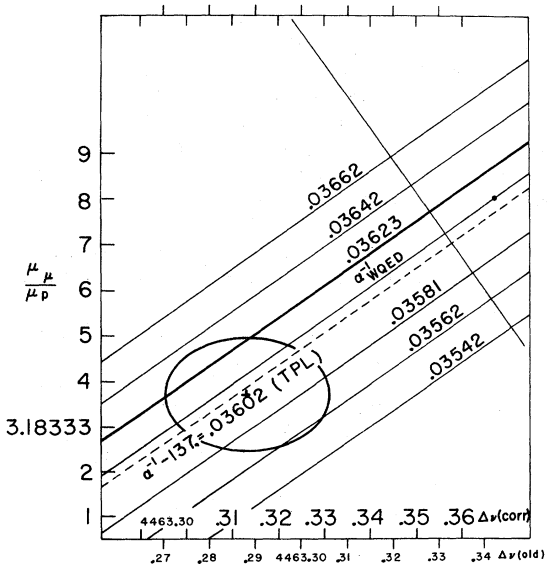

FIG. 17. Values of α^{-1} are presented for given values of μ_μ/μ_p and $\Delta\nu$. The scale $\Delta\nu$(corr) includes the Fulton-Owen-Repko correction (Ref. 7), while $\Delta\nu$(old) does not. Note that the $\Delta\nu$ value from this experiment with μ_μ/μ_p from Ref. 9 determines a value of α^{-1} in good agreement with the recommended TPL value. The graphed point is plotted using the $\Delta\nu$(corr) scale.

that of Ref. 16 [$\mu_\mu/\mu_p = 3.183\,347\,(9)$]. Equation (16) and either of these values of μ_μ/μ_p allow a determination of α. The University of Chicago μ_μ/μ_p value yields $\alpha^{-1} = 137.03595$, while the Seattle-LRL value gives $\alpha^{-1} = 137.03617$. As may be seen from Fig. 17, both these values are in good agreement with the "official"[22] α^{-1} without quantum electrodynamics, which is $\alpha^{-1}_{\mathrm{WQED}} = 137.03608\ (26)$.

Note also that, using the best value[22] of μ_μ/μ_p available at the conclusion of this experiment i. e., 3.18338 (4), the error bar this value would have included the upper three quarters of Fig. 17.

ACKNOWLEDGMENTS

This experiment was made possible through the generosity of many individuals and companies. We are indebted to Professor R. H. Hildebrand for loaning us his magnet, to Dr. E. L. Ginzton (Varian Associates) for a 4K3SJ klystron and several precision oscillators, to Mr. W. Hewlett (Hewlett-Packard Co.) for assorted microwave equipment, to Dr. G. Megla (Corning Glass Works), and Professor Ed Condon (University of Colorado) for the rf cavity, and to Dr. D. B. Sinclair (General Radio Corp.) for a general purpose oscillator. We wish to thank Professor V. W. Hughes, Professor J. Rothberg, and T. Crane of Yale for many helpful discussions, and Dr. David Fryberger (Stanford Linear Accelerator Center) and Dr. D. A. Jensen for active participation in the design phase of the experiment.

---

*Research supported at the University of Chicago by the National Science Foundation under Grant No. GP 6135.

†Present address: Yale University, New Haven, Conn.

‡Present address: Universitat Bern, Physikalisches Institut, Bern, Switzerland.

§Present address: CERN, Saclay, France.

‖ Paper submitted by D. Y. Stowell to the Department of Physics, The University of Chicago, in partial fulfillment of the requirement for the Ph. D. degree.

**Present address: University of California, San Diego, La Jolla, Cal.

[1]V. W. Hughes, Ann. Rev. Nucl. Sci. 16, 445 (1966).

[2]W. E. Cleland, thesis (Yale 1964) (unpublished).

[3]W. E. Cleland, J. M. Bailey, M. Eckhause, V. W. Hughes, R. M. Mobley, R. Prepost, and J. E. Rothberg, Phys. Rev. Letters, 13, 202 (1962).

[4]P. A. Thompson, J. J. Amato, P. Crane, V. W. Hughes, R. M. Mobley, G. zu Putlitz, and J. E. Rothberg, Phys. Rev. Letters 22, 163 (1969).

[5]P. Crane, J. J. Amato, V. W. Hughes, D. M. Lazarus, G. zu Putlitz, and P. A. Thompson, in *High Energy Physics and Nuclear Structure*, edited by S. Devons (Plenum, New York, 1970), p. 677.

[6]V. L. Telegdi, in *Proceedings of the Conference on Intermediate Energy Physics*, 1966 (College of William and Mary, Williamsburg, Va., 1966), p. 407.

[7]T. Fulton, D. A. Owen, and W. W. Repko, Phys. Rev. Letters 26, 61 (1971).

[8]T. Myint, D. Kleppner, N. F. Ramsey, and H. G. Robinson, Phys. Rev. Letters 17, 405 (1966).

[9]R. DeVoe, P. M. McIntyre, A. Magnon, D. Y. Stowell, R. A. Swanson, and V. L. Telegdi, Phys. Rev. Letters 25, 1779 (1970).

[10]D. P. Hutchinson, J. Menes, G. Shapiro, and A. M. Patlach, Phys. Rev. 131, 1351 (1969).

[11]C. Bouchiat and L. Michel, Phys. Rev. 106, 170 (1957).

[12]R. A. Swanson, Rev. Sci. Instr. 31, 149 (1960).

[13]G. Culligan, H. Hinterberger, H. Overas, V. L. Telegdi, and R. Winston, National Aeronautics and Space Administration Report No. NASA CR56934, 1964, p. 237 (unpublished).

[14]This pressure was erroneously quoted as 1.23×10^4 Torr by R. D. Ehrlich, H. Hofer, A. Magnon, D. Y. Stowell, R. A. Swanson, and V. L. Telegdi, [Phys. Rev. Letters 23, 513 (1969)]. Gauge rather than true pressure had inadvertently been used for this datum point.

[15]R. M. Herman, Phys. Rev. 136, A1576 (1964).

[16]J. F. Hague, J. E. Rothberg, A. Schenck, D. L. Williams, R. W. Williams, K. K. Young, and K. M. Crowe, Phys. Rev. Letters 25, 628 (1970).

[17]R. A. Brown and F. M. Pipkin, Phys. Rev. 174, 48 (1968).

[18]G. A. Clarke, J. Chem. Phys. 36, 221 (1962).

[19]After we presented the above argument in a preliminary version of the present work (Ref. 14), the Yale group extended their work to lower pressures and concluded that the pressure shift in argon is indeed nonlinear. This result has been reported in the Proceedings of the International Conference on Precision Measurements and Fundamental Constants, Gaithersburg, Md., 1970 (unpublished).

[20]E. S. Ensberg and C. L. Morgan, Phys. Letters 28A, 106 (1968).

[21]S. B. Crampton, D. Kleppner, and N. F. Ramsey, Phys. Rev. Letters 11, 338 (1963).

[22]W. H. Parker, B. N. Taylor, and D. N. Langenberg, Rev. Mod. Phys. 41, 375 (1969).